cw Conical Emission: First Comparison and Agreement between Theory and Experiment

J. F. Valley, G. Khitrova, H. M. Gibbs, J. W. Grantham, and Xu Jiajin
Optical Sciences Center, University of Arizona, Tucson, Arizona 85721
(Received 10 October 1989)

Experimentally observed near-field and far-field spatial profiles, frequency spectra, and cone angles are in good agreement with numerical computations of a theory that includes Doppler-broadened Raman-gain amplification of Doppler-broadened resonance fluorescence, four-wave mixing, propagational coupling, self-trapping of the pump beam, and diffraction and pump-induced refraction of the new frequencies. The use of a cw laser beam detuned from resonance by only a few gigahertz makes the computational problem tractable, leading to a simple physical model of this spatiotemporal instability.

PACS numbers: 42.50.Qg, 42.65.−k

Since its first observation by Grischkowsky,[1] conical emission has had a complicated and controversial history[2,3] with many theoretical speculations but no meaningful comparison between observations and computations. In contrast, we have excellent agreement between experimental observations and computations based on a complicated interplay of several well-known effects working simultaneously. And yet the details of the comparison do not obscure the simplicity of the physics. This understanding of conical emission that occurs in one-pass propagation is essential to further advances in the study of spatiotemporal instabilities in atomic vapors and may also have technical implications wherever intense beams must be tuned close to resonances, e.g., for isotope separation (generation of new frequencies in new directions may be important).

Our experiment makes use of a cw ring dye laser tuned to the high-frequency side of the D_2 resonance of sodium. The $\simeq$850-mW single-mode output power of the dye laser is spatially filtered, collimated, and focused by a 30-cm focal-length lens onto the cell entrance with a waist $w_0 \simeq 75$ μm and with a maximum of 600 mW reaching the sodium in a 10-cm evacuated quartz cell; see Fig. 1(h). The laser beam is vertically, linearly polarized and always travels horizontally. A Fabry-Pérot interferometer (flat mirrors with $R \simeq 0.98$, finesse of 100, usually $\simeq$28-GHz free spectral range) was used to study the frequency spectrum of the output beam after recollimating the beam and isolating the cell from the Fabry-Pérot interferometer with a polarizer and waveplate combination and neutral density filter. The detuning $\Delta\nu$ of the laser frequency from the atomic resonance is measured with Lamb-dip spectroscopy with zero defined as the midpoint between the two hyperfine transitions.

Our theoretical model is as follows. A strong cw pump beam $E_1(\omega_1)$, with Gaussian transverse profile, is focused onto the input of a sodium cell and is quasitrapped during its propagation through the cell.[4,5] New frequencies, $E_3(\omega_3)$ with $\omega_3 > \omega_1$, are generated by a Raman gain[6-11] that amplifies resonance fluorescence.[12] Additional frequencies, $E_4(\omega_4)$ with $\omega_4 = 2\omega_1 - \omega_3 < \omega_1$, are generated by propagational four-wave mixing.[8] With $E_i(x,y,z,\omega_i) = A_i(x,y,z,\omega_i)e^{i(k_i z - \omega_i t)}$, self-trapping of $A_1(x,y,z)$ is described in the paraxial and slowly varying envelope approximations by

$$\nabla_T^2 A_1 + 2ik_1 \partial A_1/\partial z = -\alpha_1 A_1 . \quad (1)$$

The equations for the interaction between weak fields A_3 and A_4 and for copropagational four-wave mixing are

$$\nabla_T^2 A_3 + 2ik_3 \partial A_3/\partial z = -\alpha_3 A_3 + \kappa_3 A_4^* + \beta_3 , \quad (2)$$

$$\nabla_T^2 A_4 + 2ik_4 \partial A_4/\partial z = -\alpha_4 A_4 + \kappa_4 A_3^* + \beta_4 , \quad (3)$$

where $k_i = 2\pi\omega_i/c$, $\nabla_T^2 = \partial^2/\partial x^2 + \partial^2/\partial y^2$, $\alpha_i(x,y,z)$ and $\kappa_i(x,y,z)$ are functions of $A_1(x,y,z)$, and ω_i has been integrated over the Doppler-velocity distribution.[10,13] α_i includes both absorption and gain and refraction leading to self-trapping of A_1 and transverse evolution of A_3 and A_4. κ_i describes the four-wave mixing that couples $A_3(\omega_3)$ and $A_4(\omega_4 = 2\omega_1 - \omega_3)$ as they propagate together through the cell. The transverse dependence [through $A_1(x,y,z)$] of the resonance fluorescence β_i from moving atoms is calculated for each frequency and each x,y,z using plasma-dispersion functions.[14] Its phase is chosen arbitrarily between 0 and 2π by a random-number generator at each x,y,z. Equations (1)–(3) are computed on a Cray using fast-Fourier-transform techniques,[15] with the spectrum of Fig. 1(f) requiring $\simeq$2 CPU hours.

The computed quasi-self-trapping of A_1 is summarized in Figs. 1(a)–1(c), and the good agreement with the experimental cell-exit and far-field profiles [Figs. 1(i) and 1(j)] indicates correct A_1 modeling (first done here with the inclusion of the longitudinal motion of the atoms). One finds that good conical emission occurs even though A_1 is only quasitrapped;[5] i.e., its diameter alternately contracts and expands as it propagates. Correct modeling of A_1 is essential since its magnitude determines the strengths of α_i and κ_i, and its phase determines the direction of energy transfer between A_3 and A_4 at each x,y,z. One finds from both the measurements and the computations that $A_3(\omega_3)$ never goes into a cone regardless of ω_3; this is shown in Figs. 1(d) and 1(e) for two particular frequencies. In contrast, $A_4(\omega_4)$ does form a well-defined cone at particular values of ω_4 as computed in Figs. 1(k) and 1(l) and photographed in Fig. 2(c). The computed spectrum of the new fields is shown in

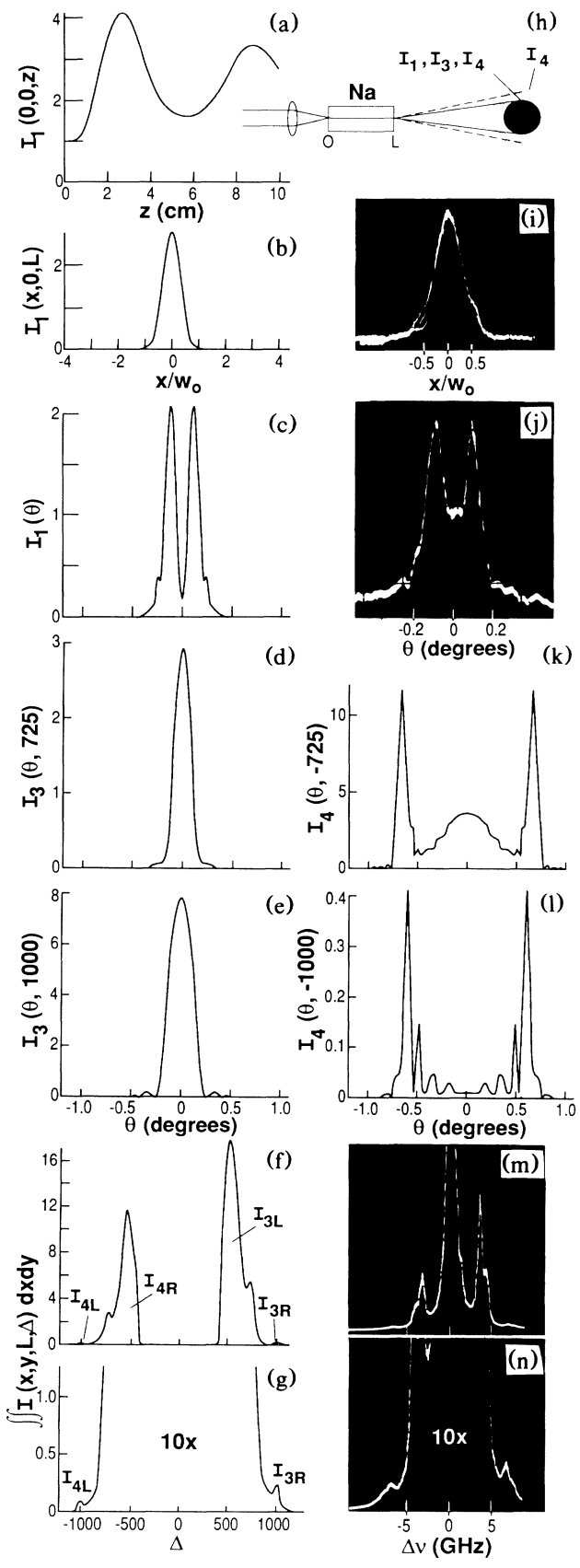

FIG. 1. Physics of cw conical emission, computed and observed. Computations: on-resonance absorption $\alpha_0 = 2300$ cm^{-1} [before Doppler broadening (Ref. 9)]; frequencies in units of $(2\pi T_1)^{-1}$ are pump detuning of +430 from the low-power atomic resonance and Rabi frequency (maximum value at the entrance of the cell) $2X = 680$; $T_2 = 2T_1$; input electric-field waist $w_0 = 72$ μm; single resonance with Doppler broadening of $ku = 105$. Experiment: pump detuning, +3.4 GHz; pump power $P = 470$ mW; $w_0 \simeq 76$ μm; $^2S_{1/2}$-$^2P_{3/2}$ D_2 transition with 1.8-GHz ground-state hyperfine transition. Computed pump beam (a) on-axis intensity, (b) near-field profile (cell-exit waist is $3.75w_0$ in absence of sodium), and (c) far-field profile. Computed far-field profiles at probe detunings Δ from the pump of (d) 725 and (e) 1000. (f),(g) Computed spectrum of new frequencies generated by Raman-gain amplification of resonance fluorescence along with four-wave mixing. (h) Schematic of setup. Observed pump beam profiles: (i) near field (cell-exit waist is $3.6w_0$ in absence of sodium); (j) far field. Computed far-field profiles at (k) $\Delta = -725$; (l) $\Delta = -1000$. (m),(n) Observed spectrum with (n) magnified 10×.

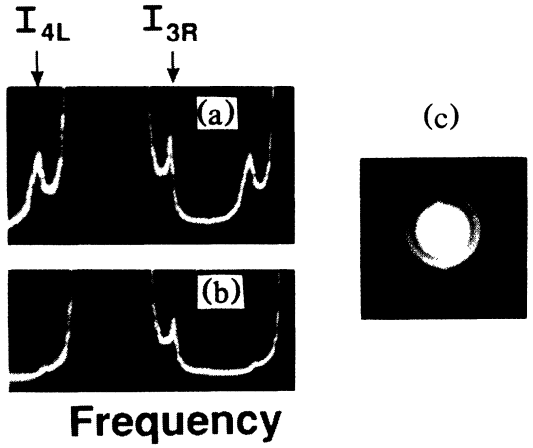

FIG. 2. I_{4L} and I_{3R} spectra with the cone (a) unblocked and (b) blocked, showing that almost all of I_{4L} goes into the cone. (c) Photograph of cone with ≃100× more intense center overexposed.

Figs. 1(f) and 1(g) and the experimental spectrum is shown in Figs. 1(m) and 1(n). Figure 2(a) shows I_{4L} and I_{3R} spectral peaks; blocking the cone [Fig. 2(b)] largely eliminates I_{4L} while hardly affecting I_{3R}. Reducing the power (Fig. 3) gives a distinctly different far-field profile, but the cone is still present and the spectrum is similar as well.

From the excellent qualitative[16] agreement between computations and experimental observations one understands the *physics of cw conical emission* as follows: self-trapping of A_1, probe generation by resonance fluorescence; Raman-gain amplification of this probe producing $A_3(\omega_3)$; four-wave mixing between $A_1(\omega_1)$ and $A_3(\omega_3)$ generating $A_4(\omega_4 = 2\omega_1 - \omega_3)$ and transferring energy back and forth between A_3 and A_4; division of A_4 into A_{4L} and A_{4R} by optical-Stark-shifted absorp-

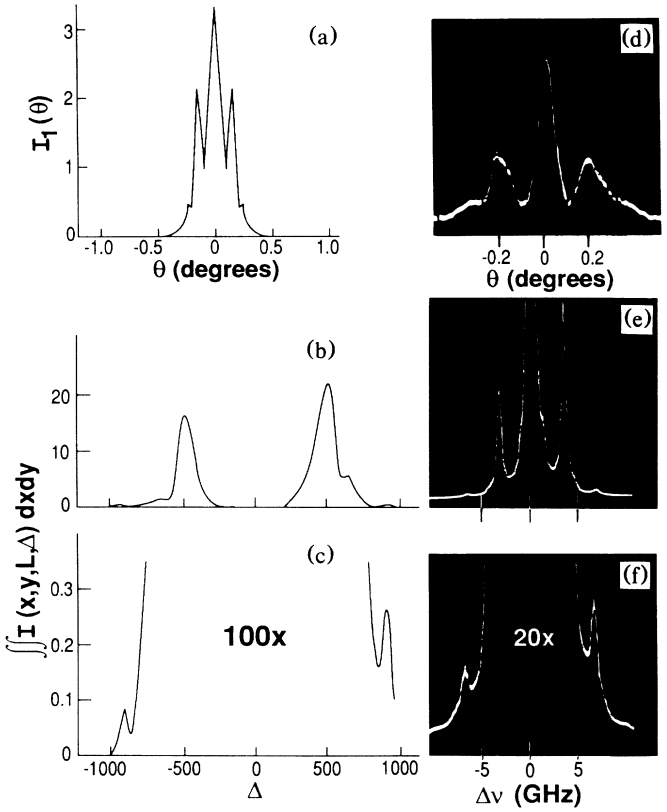

FIG. 3. Same as Fig. 1 except $2X=580$ and $P=410$ mW. Computed (a) pump-beam far-field profile and (b),(c) spectrum. Observed (d) far-field profile [peak here is 1.6× larger than the peaks in Fig. 1(j)] and (e),(f) spectrum with (f) magnified 20×.

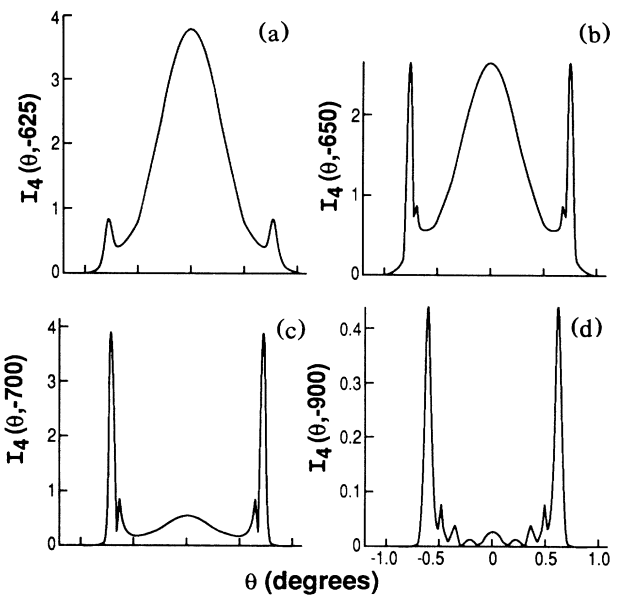

FIG. 4. Computed I_4 far-field profiles (same conditions as Fig. 3) showing that the ratio of cone power to core power increases with (a) $\Delta=-625$, (b) -650, (c) -700, and (d) -900. This qualitative behavior is observed experimentally.

tion; division of A_3 into A_{3L} and A_{3R} by four-wave-mixing coupling; and formation of the cone from A_{4L} (and sometimes from the low-energy shoulder of A_{4R}) by propagation through the spatially dependent index of refraction $\mathrm{Im}\alpha_4(x,y,z)$ prepared by $A_1(x,y,z)$. The physics of pulsed conical emission is no doubt the same except that additional frequency-generation mechanisms may contribute.

Some of the cone frequencies also appear in the center of the far-field profile, as computed in Fig. 1(k) and observed in the laboratory by examining the spatial profile of the light through the Fabry-Pérot interferometer. Figures 4(a) and 4(b) illustrate again that the same frequencies can occur in the cone and in the center, ruling out phase matching as the determinant of the cone angle, unlike many other cones, e.g., two-wavelength conical emission.[17] Also the fact that A_1 may be focusing and diffracting as it propagates [see Fig. 1(a)] implies that $\mathbf{k}_1$ depends on x, y, and z. Unlike plane-wave treatments, phase matching does not need to be imposed externally because the interference between the fields is taken care of automatically in Eqs. (2) and (3), and the transverse degrees of freedom allow phase matching to occur naturally. If one calculates the plane-wave spectrum (without ∇_T^2), one must arbitrarily impose nearly zero-phase mismatch to obtain a similar spectrum.[13]

Reduction of the power to 360 mW changes $I_1(\theta)$ to a single spike on a low pedestal and the frequency spectrum is similar to Figs. 3(b) and 3(c) with reduced shoulders on I_{4R} and I_{3L}. In the range 160–180 mW, both the computations and data show a cone from I_{4L} with sharp boundaries that expand as the power is reduced; the spectrum shows no I_{3R} peak and I_{4L} is much weaker than for Figs. 1 and 3.

Without attempting completeness, we now discuss our work in relation to previous work. Tam[18] observed a very similar cw conical emission arising from amplification of other laser odes. Harter and Boyd[8] computed the copropagation of A_3 and A_4; they did not compute the self-trapping of A_1 or include Doppler broadening, but most importantly, they did not compute the formation of the cone (i.e., they did not include ∇_T^2). Chauchard and Meyer describe but do not compute the refraction due to $A_1(x,y,z)$.[19] Gruneisen, MacDonald, and Boyd[11] have measured and computed probe gain and absorption including Doppler broadening and the Raman gain essential to cw conical emission, but because they use a small angle between A_1 and their probe A_p, the four-wave mixing at $2\omega_1-\omega_p$ is emitted at the complementary angle[13] and therefore they did not study the Doppler-broadened copropagation of A_3 and A_4. Shevy and Rosenbluh[3] have taken the best spectra of pulsed conical emission, observing the division of A_4 into A_{4L} and A_{4R} and cones from both; but they attribute the cones to two different mechanisms. At high powers, we sometimes simultaneously see a cone from A_{4L} and a

larger cone from the left shoulder of A_{4R}; we compute that both have the same origin and that A_{4R} has a larger cone angle than A_{4L} [compare Figs. 4(b) and 4(d)]. When the optical Stark shift is small, any A_{4R} that escapes the filament is absorbed by unshifted sodium atoms and only A_{4L} forms a cone. Crenshaw and Cantrell[2] have computed (with ∇_T^2) the propagation of a pulse under self-induced transparency conditions, but the 140 CPU hours required for one run prevented computations for parameters of previously pulsed conical emission experiments. cw conical emission studied here, even though necessitating the inclusion of Doppler broadening, avoids the formidable time-dependent problem of pulsed conical emission. Our approach is that of pump-probe spectroscopy or instability analyses in which the new fields, A_3 and A_4, are kept weak so that they do not affect A_1 or cause nonlinear effects themselves. Even with cw powers, we have been able to violate this assumption, generating new frequencies at $2\omega_4 - \omega_1$, etc., but that unessential complication was avoided by keeping the sodium density sufficiently low.

In summary, we have shown that cw conical emission is a spatiotemporal instability in which the cone is formed by pump-induced radially dependent refraction of new frequencies close to the Stark-shifted resonance. Previous treatments have speculated about the physics of cone generations, but here we have the first computations in excellent agreement with extensive measurements of the frequency spectra and spatial profiles.

The authors are grateful for preliminary data of M. C. Rushford, K. Tai, G. Giusfredi, and R. Pon; for helpful discussions with P. Berman, R. Boyd, E. Chauchard, D. Harter, M. LeBerre, Y. Meyer, P. R. Peterson, E. Ressayre, and A. Tallet; for research support from the U.S. Air Force Office of Scientific Research and the U.S. Army Research Office; for international travel support from the National Science Foundation (INT8612339); and for use of the Cray at Kirtland Air Force Base.

[1]D. Grischkowsky, Phys. Rev. Lett. **24**, 866 (1970).

[2]M. E. Crenshaw and C. D. Cantrell, Phys. Rev. A **39**, 126 (1989); Opt. Lett. **13**, 386 (1988).

[3]Y. Shevy and M. Rosenbluh, J. Opt. Soc. Am. B **5**, 116 (1988); Opt. Lett. **4**, 257 (1987).

[4]J. E. Bjorkholm and A. Ashkin, Phys. Rev. Lett. **32**, 129 (1974).

[5]M. L. LeBerre, E. Ressayre, A. Tallet, and F. P. Mattar, J. Opt. Soc. Am. B **2**, 956 (1985).

[6]S. Haroche and F. Hartman, Phys. Rev. A **6**, 1280 (1972).

[7]F. Y. Wu, S. Ezekiel, M. Ducloy, and B. R. Mollow, Phys. Rev. Lett. **38**, 1077 (1977).

[8]D. J. Harter, P. Narum, M. G. Raymer, and R. W. Boyd, Phys. Rev. Lett. **46**, 1192 (1981); D. J. Harter and R. W. Boyd, Phys. Rev. A **29**, 739 (1984); Opt. Lett. **7**, 491 (1982); IEEE J. Quantum Electron. **16**, 1126 (1980); R. W. Boyd, M. G. Raymer, P. Narum, and D. J. Harter, Phys. Rev. A **24**, 411 (1981).

[9]G. Khitrova, J. F. Valley, and H. M. Gibbs, Phys. Rev. Lett. **60**, 1126 (1988).

[10]G. Khitrova, P. Berman, and M. Sargent, III, J. Opt. Soc. Am. B **5**, 160 (1988).

[11]M. T. Gruneisen, K. R. MacDonald, and R. W. Boyd, J. Opt. Soc. Am. B **5**, 123 (1988).

[12]D. A. Holm, M. Sargent, III, and L. M. Hoffer, Phys. Rev. A **32**, 963 (1985).

[13]J. F. Valley, Ph.D. dissertation, Optical Sciences Center, University of Arizona, 1989 (unpublished).

[14]G. Khitrova, Xu Jiajin, and J. F. Valley (unpublished).

[15]J. V. Moloney, M. R. Belic, and H. M. Gibbs, Opt. Commun. **41**, 379 (1982), and references therein.

[16]Various approximations prevent exact quantitative agreement between the data and computations. The hyperfine structures of the $^2S_{1/2}$ ground state and $^2P_{3/2}$ excited state and optical pumping (which would require inclusion of transverse motion of the atoms in and out of the beam) were neglected. Instead the sodium was treated as a single Doppler-broadened, two-level transition. Within that approximation, the values of the detuning and Rabi frequency in GHz are obtained by dividing the normalized values in the figure captions by 100. One finds that the computed separation between peaks or absorption exceeds that observed by 30%–40%. The measured low-power, off-resonance absorption at the pump wavelength was 15% and the computation value was 7% for the conditions of Fig. 1. The measured cone angles usually exceed the computed angles by 20%. The procedure used was to adopt reasonable experimental values of α_0 and Δ and compute the far-field profiles (cones) and spectra for several Rabi frequencies within the experimental range (see Ref. 9 to relate experimental power to Rabi frequency). Then experimental data with similar far-field profiles were chosen, and the spectra were found to be in good agreement as well. Doughnut profiles like Fig. 1 were seen for powers from 430 to 500 mW, and spikes like Fig. 3 from 360 to 460 mW. Similarly, the computations show a nice doughnut for $2X = 610$–700. P and X in Figs. 1 and 3 do not scale exactly as $X \propto \sqrt{P}$, but other data or computations with equally good agreement of profiles and spectra could have been chosen that do. The important finding as one varies X is that the far-field profile of $I_1(\theta)$ changes rapidly, but the presence and angle of the cone and the overall spectrum change slowly. We conclude that, within the approximations of our model, the quantitative agreement is remarkably good and all of the qualitative features of the experimental data (dozens of recorded profiles and spectra in both 2- and 10-cm cells) also appear in the computations (about ten with uniform seed and ten with resonance-fluorescence seed).

[17]J. Krasinski, D. J. Gauthier, M. S. Malcuit, and R. W. Boyd, Opt. Commun. **54**, 241 (1985).

[18]A. C. Tam, Phys. Rev. A **19**, 1971 (1979).

[19]E. A. Chauchard and Y. H. Meyer, Opt. Commun. **52**, 141 (1984).

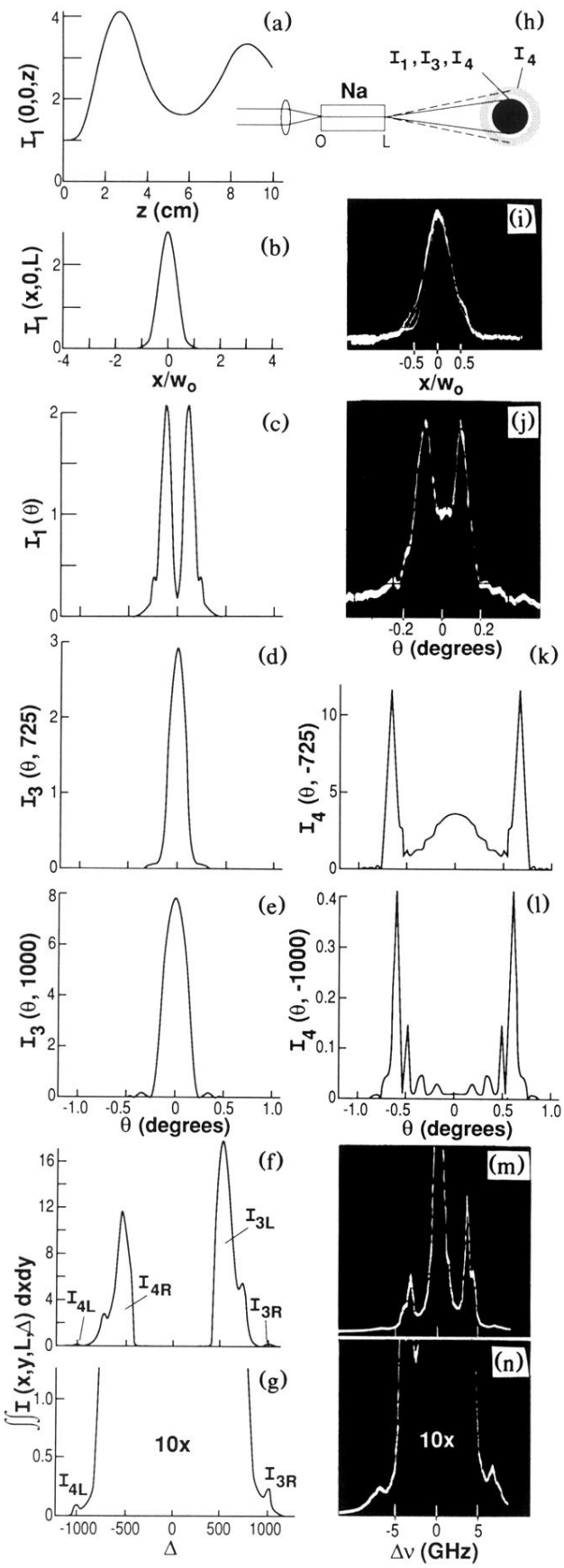

FIG. 1. Physics of cw conical emission, computed and observed. Computations: on-resonance absorption $\alpha_0 = 2300$ cm^{-1} [before Doppler broadening (Ref. 9)]; frequencies in units of $(2\pi T_1)^{-1}$ are pump detuning of $+430$ from the low-power atomic resonance and Rabi frequency (maximum value at the entrance of the cell) $2X = 680$; $T_2 = 2T_1$; input electric-field waist $w_0 = 72$ μm; single resonance with Doppler broadening of $ku = 105$. Experiment: pump detuning, $+3.4$ GHz; pump power $P = 470$ mW; $w_0 \simeq 76$ μm; $^2S_{1/2}$-$^2P_{3/2}$ D_2 transition with 1.8-GHz ground-state hyperfine transition. Computed pump beam (a) on-axis intensity, (b) near-field profile (cell-exit waist is $3.75w_0$ in absence of sodium), and (c) far-field profile. Computed far-field profiles at probe detunings Δ from the pump of (d) 725 and (e) 1000. (f),(g) Computed spectrum of new frequencies generated by Raman-gain amplification of resonance fluorescence along with four-wave mixing. (h) Schematic of setup. Observed pump beam profiles: (i) near field (cell-exit waist is $3.6w_0$ in absence of sodium); (j) far field. Computed far-field profiles at (k) $\Delta = -725$; (l) $\Delta = -1000$. (m),(n) Observed spectrum with (n) magnified 10×.

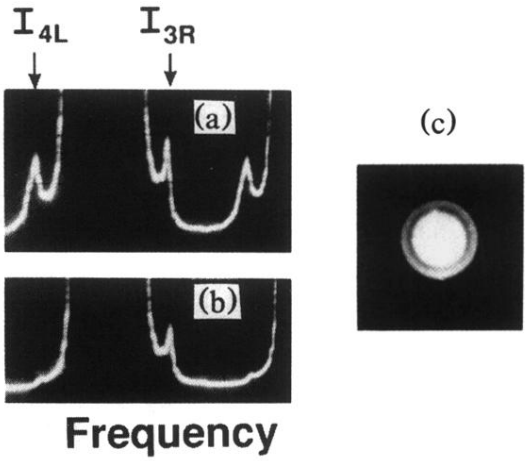

FIG. 2. I_{4L} and I_{3R} spectra with the cone (a) unblocked and (b) blocked, showing that almost all of I_{4L} goes into the cone. (c) Photograph of cone with $\simeq 100\times$ more intense center overexposed.

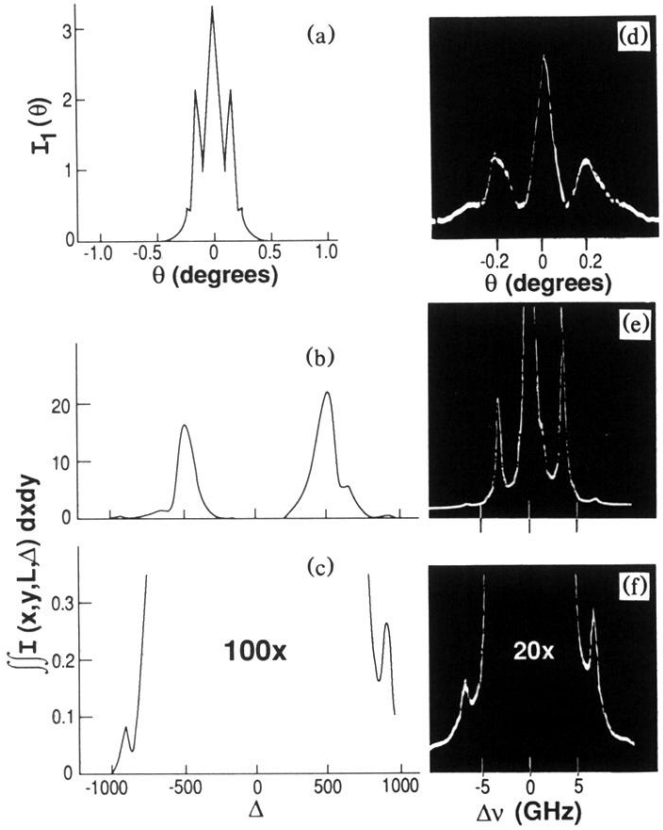

FIG. 3. Same as Fig. 1 except $2X=580$ and $P=410$ mW. Computed (a) pump-beam far-field profile and (b),(c) spectrum. Observed (d) far-field profile [peak here is 1.6× larger than the peaks in Fig. 1(j)] and (e),(f) spectrum with (f) magnified 20×.